nature climate change

LETTERS

PUBLISHED ONLINE: 31 MARCH 2013 | DOI: 10.1038/NCLIMATE1857

Asymmetric forcing from stratospheric aerosols impacts Sahelian rainfall

Jim M. Haywood[1,2]*, Andy Jones[1], Nicolas Bellouin[1†] and David Stephenson[2]

The Sahelian drought of the 1970s–1990s was one of the largest humanitarian disasters of the past 50 years, causing up to 250,000 deaths and creating 10 million refugees[1]. It has been attributed to natural variability[2–5], overgrazing[6] and the impact of industrial emissions of sulphur dioxide[7,8]. Each mechanism can influence the Atlantic sea surface temperature gradient, which is strongly coupled to Sahelian precipitation[2,3]. We suggest that sporadic volcanic eruptions in the Northern Hemisphere also strongly influence this gradient and cause Sahelian drought. Using de-trended observations from 1900 to 2010, we show that three of the four driest Sahelian summers were preceded by substantial Northern Hemisphere volcanic eruptions. We use a state-of-the-art coupled global atmosphere–ocean model to simulate both episodic volcanic eruptions and geoengineering by continuous deliberate injection into the stratosphere. In either case, large asymmetric stratospheric aerosol loadings concentrated in the Northern Hemisphere are a harbinger of Sahelian drought whereas those concentrated in the Southern Hemisphere induce a greening of the Sahel. Further studies of the detailed regional impacts on the Sahel and other vulnerable areas are required to inform policymakers in developing careful consensual global governance before any practical solar radiation management geoengineering scheme is implemented.

Atlantic sea surface temperature gradients strongly influence the position of the intertropical convergence zone (ITCZ), the Hadley cell and inflow of moisture laden air from the Gulf of Guinea into the interior of the African continent during the African monsoon. Previous studies[2–8], and others using the HadGEM climate model[9], suggest that the ITCZ moves away from the cooler hemisphere, shifting the monsoon circulation. We de-trend observational Sahelian precipitation anomalies[10,11] (SPAs) to remove the signal of multi-decadal mechanisms[3–8] to isolate the inter-annual impact of volcanic eruptions. Using the HadGEM2-ES climate model we perform simulations where stratospheric aerosol loadings are enhanced either globally or preferentially in the Northern or Southern Hemispheres to mimic volcanic eruptions and assess the impact on the modelled SPAs. As deliberate stratospheric injection has recently been suggested as a plausible climate engineering (geoengineering) measure to counterbalance predicted global warming, we also perform model simulations where emissions are made on a continual basis across both hemispheres or into each hemisphere to simulate potential global and more unilateral geoengineering scenarios (see Methods).

Figure 1a shows the time series of observed SPAs for 1900–2010[10,11] together with a robust local trend estimate (locally weighted scatter-plot smoothing[12]) and the difference in reconstructed stratospheric aerosol optical depth (AOD) between the Southern and Northern Hemispheres (AOD_{SH-NH}; refs 13,14).

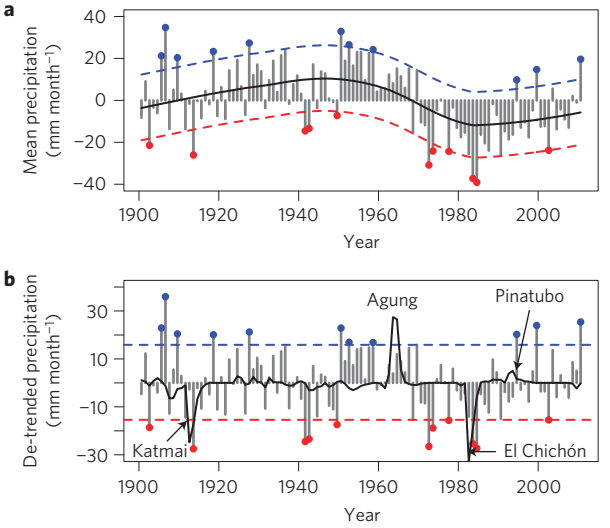

Figure 1 | Observational analysis of SPAs. a, The SPA during the June–October monsoon over the area 10°–20° N, 20° W–10° E (ref. 17). The local trend (local weighted scatter-plot smoothing[13,14]) and positive and negative 10-year return period values are shown by the solid and dashed red and blue curves; red and blue points are outside the 10-year return period value. **b**, The de-trended SPAs and black line representing $250(AOD_{SH-NH})$. The large eruptions of Katmai (peak $AOD_{NH} = 0.08$, $AOD_{SH} = 0.0$), Agung (peak $AOD_{NH} = 0.04$, $AOD_{SH} = 0.14$), El Chichón (peak $AOD_{NH} = 0.13$, $AOD_{SH} = 0.06$) and Pinatubo (peak $AOD_{NH} = 0.17$, $AOD_{SH} = 0.13$; ref. 15) are marked.

Figure 1a shows significant decadal variability and evidence of the prolonged drought in the 1980s[2,6]. The four largest de-trended negative SPAs are in 1913 (–27.5 mm month^{-1}), 1984 (–27.3 mm month^{-1}), 1972 (–26.5 mm month^{-1}) and 1983 (–25.4 mm month^{-1}). Three of these years are subsequent to eruptions of Katmai (58.28° N, Alaska, June 1912) and El Chichón (17.36° N, Mexico, April 1982), which preferentially loaded the Northern Hemisphere stratosphere. Both rainfall data and Niger and Nile river flow data have previously been used to suggest that Sahelian droughts occur subsequent to these eruptions above and beyond what would be expected from concurrently occurring El Niños[15,16]. Note that there is considerable debate about the influence of El Niños on SPAs (ref. 17) and whereas

[1]Met Office Hadley Centre, FitzRoy Road, Exeter EX1 3PB, UK, [2]CEMPS, University of Exeter, Exeter EX4 4QF, UK. †Present address: Department of Meteorology, University of Reading, Reading RG6 6BB, UK. *e-mail: j.m.haywood@exeter.ac.uk.

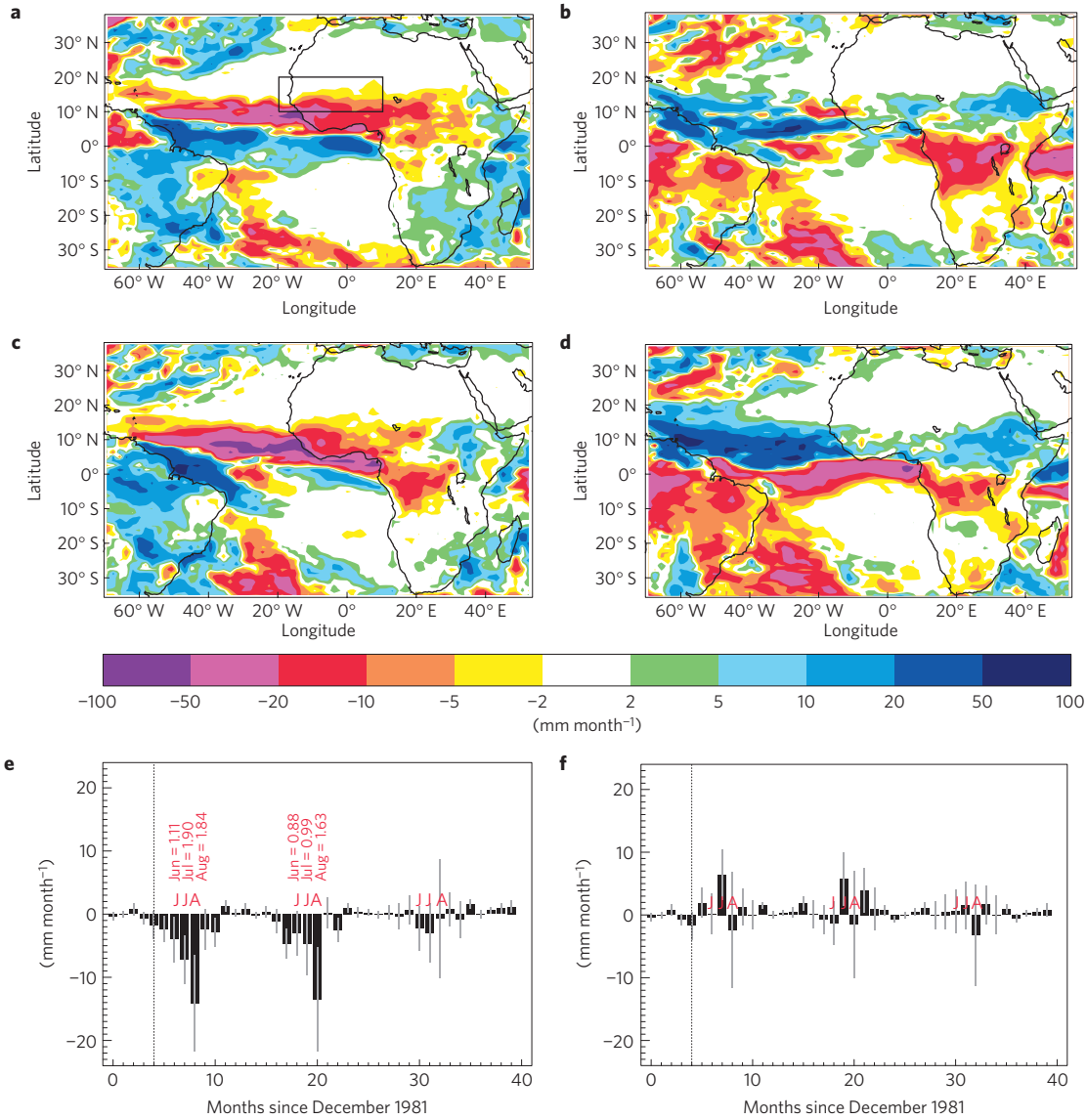

Figure 2 | Model precipitation response to volcanic simulations. a–d, Distribution of June–October mean precipitation anomaly (colour scale) compared with control simulation using means from 10-member ensembles for ECNH–control (year 1; **a**), ECSH–control (year 1; **b**), ECNH–control (year 2; **c**) and ECSH–control (year 2; **d**). The geographic area 10°–20° N, 20° W–10° E corresponding to the observation area is shown by the rectangle in **a**. **e**,**f**, The temporal evolution of the precipitation anomalies for ECNH–control (**e**) and ECSH–control (**f**); dotted lines indicate the month of eruption, and whiskers represent the mean ± 1 s.d. The numbers in **e** represent the statistical significance (standard deviations) of the SPAs in June–August.

a significant El Niño occurred concurrently with the El Chichón eruption, the Southern Oscillation was in a neutral phase during the Katmai eruption. There is no statistically significant SPA (with respect to the 10-year return period) subsequent to the eruption of Agung in 1963, which preferentially loaded the Southern Hemisphere stratosphere, or subsequent to the hemispherically symmetric eruption of Pinatubo in 1991. Although correlation does not prove causality and the sparsity of significant hemispherically asymmetric volcanic eruptions in the recent historical record hampers definitive attribution as other sources of variability are certainly present, these results provide a basis for investigating the impact of volcanic eruptions in a state-of-the-art climate model.

The observed relationship between Atlantic sea surface temperatures and SPAs seems robust in HadGEM2-ES (Supplementary Fig. S1), suggesting that any modelled volcanic-induced Northern Hemisphere cooling should lead to corresponding SPA drought. We examine the mechanistic behaviour of the HadGEM2-ES model by performing a 10-member ensemble simulation of the April 1982 El Chichón eruption using stratospheric AOD from observations[13,14] where each ensemble member has different initial conditions (ECNH). We also invert the AOD distribution to produce a 10-member ensemble simulation (ECSH) where aerosols are primarily distributed in the Southern Hemisphere, a 10-member ensemble simulation where an identical stratospheric AOD is distributed in the same latitudinal bands, but in both hemispheres (ECG), and a 10-member ensemble of the Katmai eruption (see Methods). The spatial distribution and temporal evolution of the SPAs for ECNH and ECSH are shown in Fig. 2 (see Supplementary Fig. S2 for ECG).

For ECNH, Fig. 2a,c shows a clear shift of the ITCZ to the south for the two years after the Northern Hemisphere eruption as evidenced by the latitudinal dipole in the precipitation anomaly across the Atlantic and into the interior of the African continent.

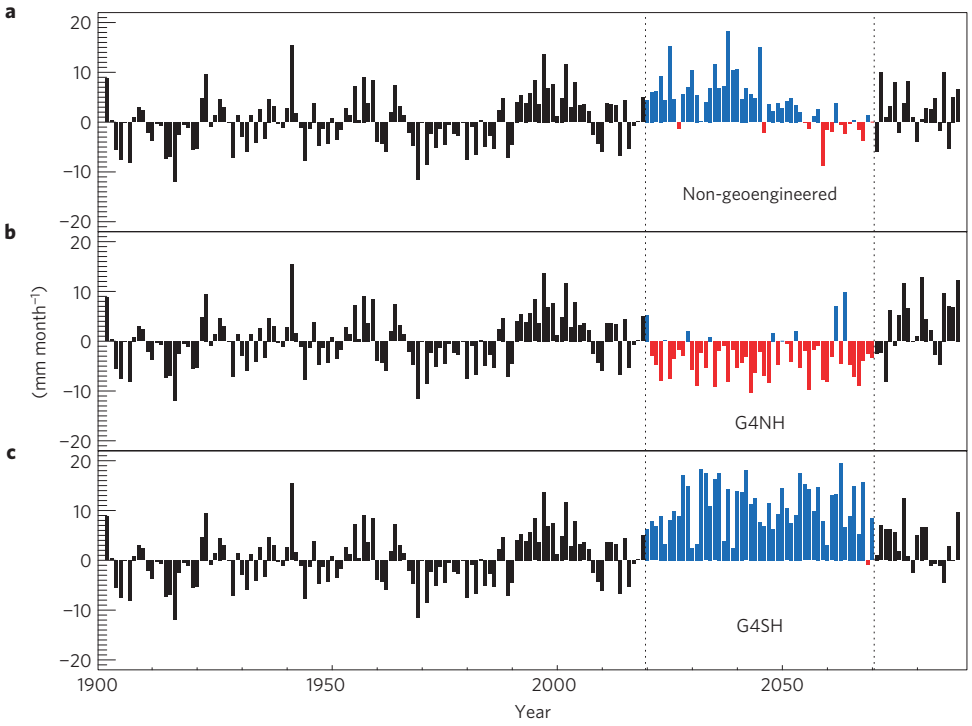

Figure 3 | The June–October SPA in HadGEM2 as a function of year over the geographic area 10°–20° N, 20° W–10° E. Simulations use historical forcings before 2005 followed by a business-as-usual (RCP4.5; ref. 31) simulation for 2005–2020. **a**–**c**, For the years 2020–2070, the simulations correspond to the non-geoengineered scenario (**a**), G4NH (**b**) and G4SH (**c**). The period 2020–2070 is highlighted by the red and blue bars. In 2070, geoengineering is terminated.

For ECSH, Fig. 2b,d shows a less clear picture: although the dipole is reversed across the Atlantic as might be expected from the premise that the ITCZ moves away from the cooler hemisphere, the signal over the Sahelian region is weaker than for ECNH and not generally significant (at 1 s.d.). Figure 2e shows that, for ECNH, the SPA drought is significantly different from zero during the first year at between 1.1 and 1.9 s.d. (or 86–97% confidence). The magnitude of the modelled mean SPA drought can exceed −13 mm per month during the peak of the monsoon for the first and second years subsequent to the simulated eruption. The mean June–October seasonal SPA is –6.1 mm for year 1 and –4.7 mm for year 2. If we account for the underestimation of the seasonal SPA in the model utilizing the ratio of the slopes of observed and modelled SPA/sea surface temperature anomaly (SSTA; Supplementary Fig. S1) we might expect an SPA drought of 21–27 mm, which is in agreement with the observations (Fig. 1). By year 3, when the stratospheric aerosol loading has returned to pre-eruption values there is no discernible SPA. Figure 2f shows that, for ECSH, commensurate with the weaker spatial signature shown in Fig. 2c,d, the modelled mean SPA is more difficult to identify. The SPAs from the volcanic simulations are consistent with the observations shown in Fig. 1: a volcanic eruption into the Northern Hemisphere of the magnitude of El Chichón can lead to Sahelian drought. To a lesser extent, a volcanic eruption into the Southern Hemisphere can lead to an increase in Sahelian rainfall, but this is unlikely to be statistically significant (at 1 s.d.). ECG simulations shows less evidence of Sahelian drought than ECNH simulations because the model simulation from ECG is very similar to the mean of the ECNH and ECSH simulations (Supplementary Fig. S2). Simulations for the Katmai eruption show no statistically significant SPA during 1912 (at 1 s.d.), but the Sahelian drought is significantly different from zero at around 2.3 and 2 s.d. (or 99% and 98% confidence) during July and August 1913 when the geographical distribution of precipitation anomaly is very similar to that from ECNH simulations (Supplementary Fig. S3). Thus, the observed Sahelian droughts in 1913, 1982 and 1983 are all reproduced in the model.

Climate engineering (geoengineering) to deliberately cool the Earth has recently been suggested as a plausible measure to counterbalance the predicted global warming caused by mankind's continued reliance on fossil fuels, although there are, of course, concerns associated with any such approach[18,19]. One plausible scheme is the injection of sulphur dioxide into the stratosphere to mimic the climatic impacts of a large volcanic eruption[20–22]. The most comprehensive multi-model simulations so far have frequently been based on the production of a globally uniform layer of aerosol or on a dimming of the sun[23,24], although there have been suggestions that high-latitude regions could be targeted to maintain levels of sea ice[22,25,26]. Using HadGEM2-ES we perform and analyse two experiments that are variants of the Geoengineering Model Intercomparison Project G4 experiment[23]; we call these G4NH and G4SH, where injections of 5 T gSO_2 yr^{-1} were made into the Northern and Southern Hemispheres only for 2020–2070 (see Methods).

Under both G4NH and G4SH scenarios, AOD at 550 nm reaches a steady state with a global perturbation of around 0.05 after around 5 years. The AOD is meridionally well mixed with around 85% distributed in the Northern/Southern Hemisphere for G4NH/G4SH, respectively (Supplementary Fig. S4). The isolation between the hemispheres is a well-documented feature of the Brewer–Dobson circulation. The AOD in the geoengineering simulations is thus around half of the peak stratospheric AOD in the El Chichón volcanic simulations (Fig. 1, caption), but is sustained throughout a 50-year period. As in the G4 simulation, the G4NH and G4SH simulations exhibit a global

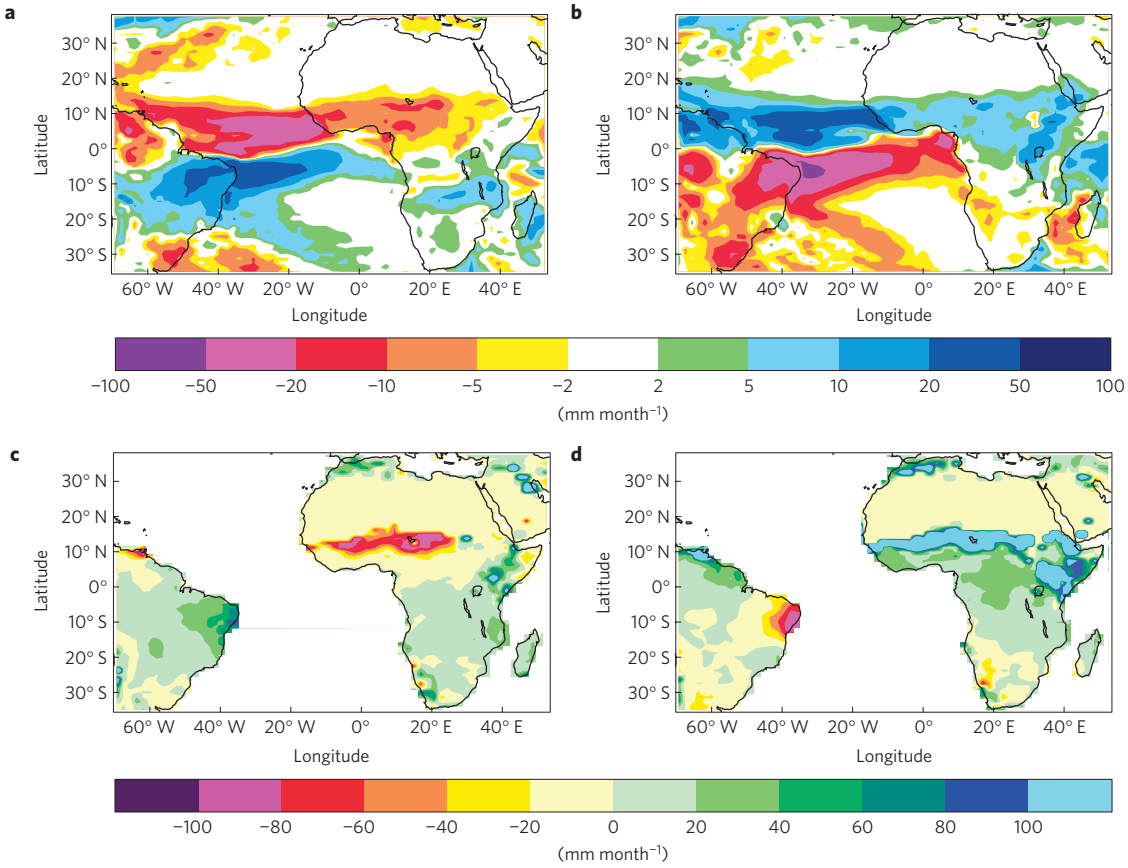

Figure 4 | Model precipitation and NPP response to geoengineering simulations. a,**b**, The change in annual mean precipitation (colour scale) averaged over the period 2020–2070 for G4NH (**a**) and G4SH (**b**). **c**,**d**, The percentage change (colour scale) in the NPP over the period 2020–2070 under G4NH (**c**) and G4SH (**d**). Areas where the absolute NPP in the non-geoengineered simulation is negligible (less than 1×10^{-3} kg C m^{-2} yr^{-1}) are removed for clarity.

cooling over the geoengineering period of –0.70 to –0.80 K, demonstrating the potential effectiveness of stratospheric geoengineering in reducing global warming. The temporal evolution of the SPAs is shown in Fig. 3.

Figure 3 shows that under the non-geoengineered scenario the SPA continues to be generally positive until 2090 with only 11 out of 50 years during the period 2020–2070 showing negative values. The modelled increase in Sahelian precipitation is due to the Northern Hemisphere warming more than the Southern Hemisphere in the Representative Concentration Pathway (RCP)4.5 scenario. The results are radically different for G4NH, where 44 out of 50 years show negative values during the period 2020–2070. Subsequent to 2070, when G4NH geoengineering is terminated, SPAs recover and resemble those of the non-geoengineered scenarios. For G4SH, geoengineering increases the SPA with only 1 out of 50 years showing a negative value. These results may be understood by considering the correlation between the SPA and the SSTA, which seems to be robust (Supplementary Fig. S5), noting that the sensitivity in the model is smaller than in the observations and the model is therefore more likely to underestimate the impacts (Supplementary Fig. S1). Using data from the mean for 2020–2070 for geoengineering simulations and the second year after the eruption for volcanic simulations, the ratio of the SSTAs for G4NH/ECNH, G4NH/Katmai and G4SH/ECSH is approximately 0.85, 0.85 and 2.8, respectively, helping explain why a clear impact on SPAs is evident for G4NH, G4SH and ECNH, but not for ECSH.

Figure 4a,b shows that the G4NH produces precipitation anomaly patterns that are strikingly similar to those for ECNH whereas those for G4SH are similar to those for ECSH (Fig. 2).

As in the hemispherically symmetric volcanic simulations, hemispherically symmetric geoengineering simulations (G4) produce SPAs that are similar to that for the mean of G4NH and G4SH (Supplementary Fig. S6c,d).

Precipitation is a key factor in agriculturally vulnerable areas such as the Sahel. HadGEM2-ES contains a coupled carbon cycle for simulating the impact on the net primary productivity (NPP equal to the gross primary productivity minus respiration), which is a key agricultural indicator. The impacts on the percentage change in NPP are shown in Fig. 4c,d. The G4NH simulation shows that the Sahelian region (Niger, Mali, Burkina Faso, Senegal, Chad and the Sudan) is subject to reductions in NPP by 60–100%, which would clearly be very detrimental. Conversely, G4SH shows that NPP is enhanced by a factor of greater than 100%, which would have clear benefits for the region. The causes of these shifts in the ITCZ and associated precipitation are geographic shifts in the position and extent of the maximum in the surface temperatures. These influence the strength and position of the Hadley cell, which is strongly coupled to African monsoon flow (see Supplementary Figs S7–S9). Note that many further observed dynamical impacts of volcanic eruptions and the fidelity of models in representing these impacts have been studied[27].

The implications from this study are far-reaching. Among other factors, significant volcanic eruptions that preferentially load the

Northern Hemisphere stratosphere increase the probability and, if large enough, may be the harbinger, of significant Sahelian drought. In a similar vein, deliberate geoengineering injections into the Northern Hemisphere will preferentially load the Northern Hemisphere stratosphere causing Sahelian drought, whereas stratospheric geoengineering in the Southern Hemisphere will cause a significant increase in Sahel vegetation productivity or a greening of the region. Deliberate stratospheric injection into the Southern Hemisphere could theoretically be instigated to increase Sahelian rainfall, ameliorate Sahelian droughts such as those experienced in the 1970s–1990s or to offset droughts caused by major Northern Hemisphere volcanic eruptions. Note, however, that on an intercontinental scale this apparent positive impact is offset by the impact in the Nordeste region of Brazil where significant reductions in rainfall and vegetation productivity are noted. Clearly, the juxtaposition of impacts leads us to believe that a global governance agreement for geoengineering is essential before any practical geoengineering system is deployed and much further research is needed into modelling the impacts of solar radiation management schemes including assessments using multi-model ensembles[23].

Methods

Observational data sets. Observational SPAs in the region 10°–20° N, 20° W–10° E are derived by subtracting the long-term mean, are available at monthly resolution and are reported in millimetres per month (refs 10,11). Observed North–South Atlantic SSTA data are derived from HADISST1 (ref. 28). June–October anomalies for 1900–2000, relative to the local calendar month average in each grid box for 1900–2000, were first averaged over June–October and then over the North and South Atlantic Ocean separately. The difference between the North and South Atlantic SSTAs is then calculated. Monthly mean reconstructed aerosol optical depths derived from measurements of solar extinction at different latitudes for the Northern and Southern Hemispheres[13,14] are obtained and the difference between the optical depths determined.

General circulation model. HadGEM2-ES (ref. 29) is a fully coupled atmosphere–ocean climate model developed by the Met Office Hadley Centre. The atmospheric component has 38 levels extending to 40 km, with a horizontal resolution of 1.25° × 1.875° latitude and longitude respectively, equivalent to a surface resolution of about 208 km × 139 km at the Equator, reducing to 120 km × 139 km at 55° latitude. ES refers to the Earth System version of the model, which includes coupling to the carbon cycle. The model includes the Coupled Large-scale Aerosol Simulator for Studies In Climate (CLASSIC) aerosol scheme[30], which represents major aerosol components and direct and indirect effects.

HadGEM2-ES is forced following the Climate Model Intercomparison Project phase 5 (CMIP5) protocol using historical data from 1860 to 2005 and RCP scenarios[31] up to 2100. Well-mixed greenhouse-gas concentrations (CO_2, CH_4, N_2O and halocarbons) are prescribed as are emissions of anthropogenic aerosols or their precursors whereas sea-salt and mineral dust aerosol emissions are simulated interactively according to climate conditions in the model[29,30]. Tropospheric ozone is simulated by the model from surface and aircraft emissions of tropospheric ozone precursors and reactive gases. Stratospheric ozone is prescribed as monthly zonal/height fields that cover the period 1850–2100. Land cover is simulated by the model's dynamic vegetation scheme but also forced by scenarios of anthropogenic land-use change to represent deforestation and changes in agricultural extent. Natural climate forcings are represented by prescribing time-varying changes in total solar irradiance and monthly volcanic perturbations to stratospheric aerosols and are applied in four equal area latitudinal bands with updates for the period 1990–2005. To represent natural forcing in the future scenarios, and to prevent a discontinuity due to a sudden change in forcing after 2005, the last solar cycle is repeated and volcanic forcing is reduced smoothly to a background value. Up until 2020, the simulations are referred to as non-geoengineered or RCP4.5 simulations.

Volcanic and geoengineering simulations. For the volcanic simulations, a control simulation was performed consisting of perpetual pre-industrial conditions. The volcanic eruption was simulated by applying a time-varying horizontal and vertical perturbation to the AOD for the period representing the eruption of El Chichón in April 1982[13,14]. The peak perturbation (global AOD at 550 nm of 0.098) is in the Northern Hemisphere in the latitude band 0–30° N and the simulation is referred to as ECNH. A second simulation was performed simply by inverting the latitudinal distribution of the perturbations from the Northern Hemisphere to the Southern Hemisphere; this is referred to as ECSH. A third simulation was also performed by averaging the AODs from ECNH and ECSH to form a globally symmetric simulation referred to as ECG. A fourth simulation was performed representing the eruption of Katmai in June 1912 using the appropriate AODs (refs 13,14); this is referred to as Katmai. Four 10-member ensembles were constructed for ECNH, ECSH, ECG and Katmai simulations, initializing each member of the ensemble at the start of December with conditions from different years of the control simulation. The simulated eruption occurs in the following April for ECNH, ECSH and ECG and in June for the Katmai simulation and data for the subsequent three boreal summers are presented as the difference between the eruption and the control simulations.

Geoengineering simulations are performed by injecting 5 Tg of SO_2 per year into the stratosphere from the year 2020 either into both hemispheres or the Northern or Southern Hemispheres across all latitude bands (experiments entitled G4, G4NH or G4SH respectively). The model contains its own sulphur cycle[30] for oxidation of sulphur dioxide to sulphate aerosol, which has been shown to compare well against observations after volcanic eruptions[32]. Geoengineering is stopped at the beginning of 2070 for all scenarios.

Received 23 October 2012; accepted 22 February 2013; published online 31 March 2013

References

1. http://www.unep.org/dewa/Africa/publications/AEO-1/056.htm.
2. Zeng, N. Drought in the Sahel. *Science* **302,** 999–1000 (2003).
3. Folland, C. K., Palmer, T. N. & Parker, D. E. Sahel rainfall and worldwide sea temperatures, 1901–85. *Nature* **320,** 602–607 (1986).
4. Chang, P *et al.* Oceanic link between abrupt changes in the North Atlantic Ocean and the African monsoon. *Nature Geosci.* **1,** 444–448 (2008).
5. Shanahan, T. M. *et al.* Atlantic forcing of persistent drought in West Africa. *Science* **324,** 377–380 (2009).
6. Charney, J. Dynamics of deserts and drought in the Sahel. *Q. J. R. Meteorol. Soc.* **101,** 193–202 (1975).
7. Booth, B. B. B., Dunstone, N. J., Halloran, P. R., Andrews, T. & Bellouin, N. Aerosols implicated as a prime driver of twentieth-century North Atlantic climate variability. *Nature* **484,** 228–232 (2012).
8. Held, I. M., Delworth, T. L., Lu, J., Findell, K. L. & Knutson, T. R. Simulation of Sahel drought in the 20th and 21st centuries. *Proc. Natl Acad. Sci. USA* **102,** 17891–17896 (2005).
9. Jones, A., Haywood, J. M. & Boucher, O. Aerosol forcing, climate response and climate sensitivity in the Hadley Centre climate model HadGEM2-AML. *J. Geophys. Res.* **112,** D20211 (2007).
10. Janowiak, J. E. An investigation of interannual rainfall variability in Africa. *J. Clim.* **1,** 240–255 (1988).
11. http://jisao.washington.edu/data/sahel
12. Cleveland, W. S. Robust locally weighted regression and smoothing scatterplots. *J. Am. Stat. Assoc.* **74,** 829–836 (1979).
13. Sato, M., Hansen, J. E., McCormick, M. P. & Pollack, J. B. Stratospheric aerosol optical depth, 1850–1990. *J. Geophys. Res.* **98,** 22987–22994 (1993).
14. http://data.giss.nasa.gov/modelforce/strataer/
15. Robock, A. & Liu, Y. The volcanic signal in Goddard Institute for Space Studies three-dimensional model simulations. *J. Clim.* **7,** 44–55 (1994).
16. Oman, L., Robock, A., Stenchikov, G. L. & Thordarson, T. High-latitude eruptions cast shadow over the African monsoon and the flow of the Nile. *Geophys. Res. Lett.* **33,** L18711 (2006).
17. Nicolson, S. E. & Kim, J. The relationship of the El Niño-Southern Oscillation to African rainfall. *Int. J. Climatol.* **17,** 117–135 (1997).
18. Robock, A. 20 reasons why geoengineering may be a bad idea. *Bull. Atom. Scient.* **64,** 14–18 (2008).
19. Lenton, T. M. & Vaughan, N. E. The radiative forcing potential of different climate geoengineering options. *Atmos. Chem. Phys.* **9,** 5539–5561.
20. Keith, D. W., Parson, E. & Morgan, M. G. Research on global sun block needed now. *Nature* **463,** 426–427 (2010).
21. Jones, A., Haywood, J. M., Boucher, O., Kravitz, B. & Robock, A. Geoengineering by stratospheric SO_2 injection: Results from the Met Office HadGEM2 climate model and comparison with the Goddard Institute for Space Studies ModelE. *Atmos. Chem. Phys.* **10,** 5999–6006 (2010).
22. Robock, A., Oman, L. & Stenchikov, G. L. Regional climate responses to geoengineering with tropical and Arctic SO_2 injection. *J. Geophys. Res.* **113,** D16101 (2008).
23. Kravitz, B. *et al.* The Geoengineering Model Intercomparison Project (GeoMIP). *Atmos. Sci. Lett.* **12,** 162–167 (2011).
24. Schmidt, H. *et al.* Solar irradiance reduction to counteract radiative forcing from a quadrupling of CO_2: Climate responses simulated by four Earth system models. *Earth Syst. Dynam.* **3,** 63–78 (2012).
25. Caldeira, K. & Wood, L. Global and Arctic climate engineering: Numerical model studies. *Phil. Trans. R. Soc. A* **366,** 4039–4056 (2008).
26. MacCracken, M.C., Shin, H-J., Caldeira, K. & Ban-Weiss, G. A. Climate response to imposed solar radiation reductions in high latitudes. *Earth Syst. Dynam. Discuss.* **3,** 715–757 (2012).

27. Stenchikov, G. *et al.* Arctic oscillation response to volcanic eruptions in the IPCC AR4 climate models. *J. Geophys. Res.* **111,** D07107 (2006).
28. Rayner, N. A. *et al.* Global analyses of sea surface temperature, sea ice, and night marine air temperature since the late nineteenth century. *J. Geophys. Res.* **108,** D14, 4407 (2003).
29. Colllins, W. J. *et al.* Development and evaluation of an Earth-system model—HadGEM2. *Geosci. Model Dev.* **4,** 1051–1075 (2011).
30. Bellouin, N., Rae, J., Jones, A., Johnson, C., Haywood, J. M. & Boucher, O. Aerosol forcing in the CMIP5 simulations by HadGEM2-ES and the role of ammonium nitrate. *J. Geophys. Res.* **116,** D20206 (2011).
31. Moss, R. H. *et al.* The next generation of scenarios for climate change research and assessment. *Nature* **463,** 747–756 (2010).
32. Haywood, J. M. *et al.* Observations of the eruption of the Sarychev volcano and simulations using the HadGEM2 climate model. *J. Geophys. Res.* **115,** D21212 (2010).

Acknowledgements

N. Rayner is thanked for providing the HadISST SSTA data. T. Mitchell is thanked for maintaining the JISAO SPA records. P. Cox and T. Lenton are thanked for their encouragement. O. Morton and J. Knight are thanked for comments regarding the content, style and presentation of the work. This work was supported by the SPICE programme (http://www2.eng.cam.ac.uk/~hemh/climate/Geoengineering_RoySoc.htm), the IAGP programme (http://www.iagp.ac.uk/) and the Joint DECC/Defra Met Office Hadley Centre Climate Programme.

Author contributions

J.M.H. came up with the idea for the experiments, analysed the experimental and model data, and wrote the paper. A.J. set up and ran the experiments, and analysed the model and observational data. N.B. performed analysis of the model and observational data. D.S. performed statistical analysis of the observational data.

Additional information

Supplementary information is available in the online version of the paper. Reprints and permissions information is available online at www.nature.com/reprints. Correspondence and requests for materials should be addressed to J.M.H.

Competing financial interests

The authors declare no competing financial interests.